🔓**Open Access**

Compact and Broadband Edge Coupler Based on Multi-Stage Silicon Nitride Tapers

Bishal Bhandari
Chul-Soon Im
Kyeong-Pyo Lee
Sung-Moon Kim
Min-Cheol Oh
Sang-Shin Lee
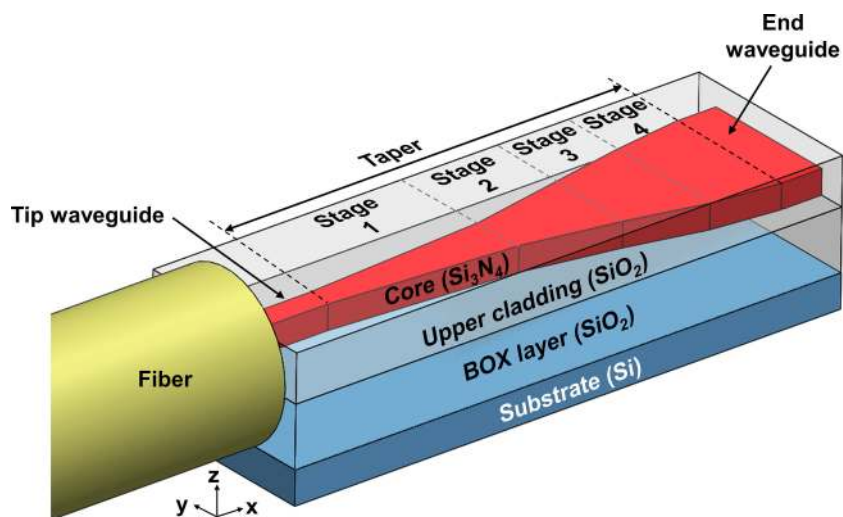
Compact and Broadband Edge Coupler Based on Multi-Stage Silicon Nitride Tapers

Bishal Bhandari [ID],[1] **Chul-Soon Im** [ID],[1] **Kyeong-Pyo Lee,**[2]
Sung-Moon Kim [ID],[3] **Min-Cheol Oh** [ID],[3] **and Sang-Shin Lee** [ID][1]

[1]Department of Electronic Engineering, Kwangwoon University, 20 Kwangwoon-ro,
Nowon-gu, Seoul 01897, South Korea
[2]i3system, 26-32 Gajeongbuk-ro, Yuseong-gu, Daejeon 34113, South Korea
[3]Department of Electronics Engineering, Pusan National University, 2 Busandaehak-ro,
63beon-gil, Geumjeong-gu, Pusan (Busan) 46241, South Korea

Abstract: We have proposed and experimentally realized an ultra-compact and broadband silicon nitride edge-coupler that enables high coupling efficiency. The proposed coupler was realized by concatenating short tapers in four stages, whose angles were designed to minimize the footprint while preserving the coupling efficiency. The constituting taper segments were designed by carefully sectioning a long adiabatic taper while adapting to an appropriate taper angle for each segment. The designed coupler exhibited an extremely short footprint of 76 μm. A coupling efficiency of 92% was experimentally attained at 1550 nm wavelength when coupled to a single-mode fiber having a mode field diameter of $\sim$4 μm. Further, an efficiency of over 90% throughout the C and L bands was observed. A 3-dB bandwidth of 965 nm, spanning $\lambda = 1015$–1980 nm, was achieved in the simulation. Additionally, the fabricated device exhibited an enhanced cleaving tolerance by virtue of its elongated tip, along with relaxed alignment tolerances ranging up to 3.5 μm. The proposed design was also found to comply with the waveguides having widths between 1 μm and 4 μm without affecting the overall footprint and efficiency. This work is anticipated to provide a promising foundation for the development of compact photonic devices.

Index Terms: Integrated optics device, silicon nitride photonics, edge coupler.

1. Introduction

With the growing prominence of high-speed and compact devices, photonic integrated circuits (PICs) have garnered considerable interest owing to their large-capacity transmission and fabrication compatibility with the existing complementary metal-oxide-semiconductor (CMOS) technology. In recent years, silicon nitride (Si$_3$N$_4$) has gained tremendous attention as a platform for PICs due to its low propagation loss, three-dimensional (3D) integration compatibility, extended transparent bandwidth, and less susceptibility to fabrication errors during lithography and etching process, as compared to silicon on insulator (SOI) platform [1]–[3]. Typically, PICs require an effective coupling mechanism for launching light into a waveguide from a fiber. To this end, grating couplers and edge couplers are widely adopted mechanisms [4]–[17]. The grating couplers are perceived to be suitable for out-of-plane coupling, exhibiting a coupling efficiency of $\sim$1 dB, yet they inherently suffer

from a limited bandwidth [4]–[7]. Compared to grating couplers, the edge couplers exhibit superior in-plane light coupling and broader spectral bandwidth. However, most of the edge couplers are designed to entail long adiabatic tapers with a length exceeding several hundred micrometers, thereby enhancing the mode transfer. Considering the adiabatic tapers exhibiting longer lengths have been deployed in applications like 2×2 couplers [18]–[22], mode multiplexers [23]–[26], and polarization splitters/rotators [27]–[30], a compact form of adiabatic taper is slated to drastically facilitate its applicability in high-density PICs [4]. In order to attain a short and efficient taper applicable for high-density PICs, various configurations like nonlinear tapers, stepwise cascaded tapers, multi-layered tapers, metamaterials as well as double-tip and sinusoidal tapers have been extensively explored in different platforms [8]–[17]. However, unlike other platforms, compact tapers for edge couplers on Si_3N_4 platform have been rarely investigated and reported in the literatures. The lower index contrast of a Si_3N_4 waveguide strictly prohibits small bend radii, constraining the realization of an edge coupler with a small footprint [3]. An adiabatic Si_3N_4 fiber-to-waveguide coupler based on a taper with a length of 500 μm was reported to attain a coupling efficiency of 98% [15]. To achieve a miniaturized coupler, a fiber-to-waveguide coupler, where two tapers with different thicknesses were appended to each other, was demonstrated to provide a coupling loss of 0.58 dB for an overall taper length of 151 μm [17]. Further, it incorporated multiple Si_3N_4 thicknesses, which might lead to increased complexity and additional cost for the fabrication process. A multi-stage taper was demonstrated for applications such as waveguide-to-waveguide and evanescent coupler in a different platform [31]. However, the realization of fiber-to-waveguide edge coupler using a multi-stage taper composed of a Si_3N_4 waveguide has never been reported. Thus, a fiber-to-waveguide edge coupler based on a low-index platform should be developed from the perspective of optimizing the reproducibility, design complexity, taper length, taper angle, and coupling efficiency [9]–[17].

In this study, we propose a substantially miniaturized Si_3N_4 edge coupler incorporating four concatenated stages, which provides high efficiency over a broad bandwidth. To minimize the footprint, the maximum acceptable taper angle corresponding to each stage was first identified for a long adiabatic taper. The long taper was subsequently superseded with a new short taper assuming a similar taper angle, providing a commensurate taper efficiency. A taper with a four-stage configuration was established with a cumulative length of 76 μm, delivering a coupling efficiency of up to 92% in the vicinity of $\lambda = 1550$ nm. The proposed coupler was designed to mimic the fundamental mode of a fiber, which exhibited an ultra-high numerical aperture (NA) of 0.35 and a mode field diameter (MFD) of $\sim$4 μm. Considering the splicing between the high-NA fiber and a standard single-mode fiber (SMF) that incurs a loss as small as 0.06 dB [32], the proposed multi-stage coupler can be readily applied to a standard SMF via a spliced high-NA fiber. Owing to its simple structure and judiciously chosen structural parameters, the proposed device can be engineered to exhibit minimal imperfections under standard fabrication facilities using a single-step fabrication process. Further, the proposed scheme facilitates a relaxed alignment tolerance as well as a broad spectral bandwidth, while requiring a substantially small footprint tantamount to half the length of the shortest case as reported in [17]. Hence, this work provides a promising foundation for the development of compact photonic devices that can aid high-density integration in PICs.

2. Design of the Proposed Multi-Stage Tapered Coupler

Fig. 1 shows a 3D illustration of the proposed coupler, where a multi-stage taper is constructed on a 500-nm thick Si_3N_4 core, placed atop a silicon substrate coated with a 4-μm thick buried oxide (BOX). A 3-μm thick SiO_2 layer acts as the upper cladding for the taper. Unlike a typical single-stage long taper based on adiabatic mode evolution, the mode evolves abruptly over four stages in the proposed device. The taper angle is properly tailored for each stage to achieve a small footprint without deteriorating the overall coupling efficiency. The tip end of the taper corresponding to Stage 1 is elongated using a tip waveguide (TWG), thereby securing flexibility in the cleaving position. Light emanating from a fiber impinges on the tip waveguide and successively advances from Stage 1 through Stage 4 reaching the 2-μm wide end waveguide (EWG).
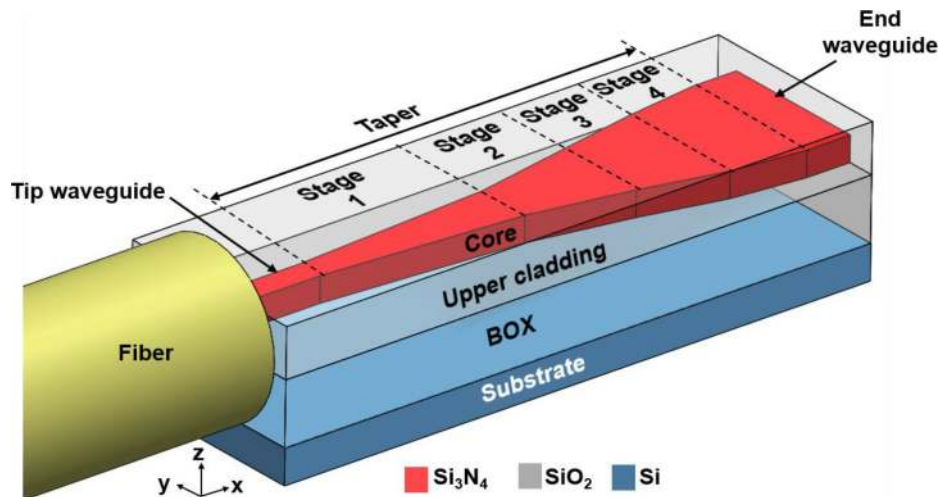
Fig. 1. (a) 3D illustration of the proposed tapered coupler comprising short taper segments forming Stage 1 through Stage 4 from the tip waveguide to the end waveguide. The tip end of the taper for Stage 1 is elongated using the tip waveguide for enhancing the cleaving tolerance.
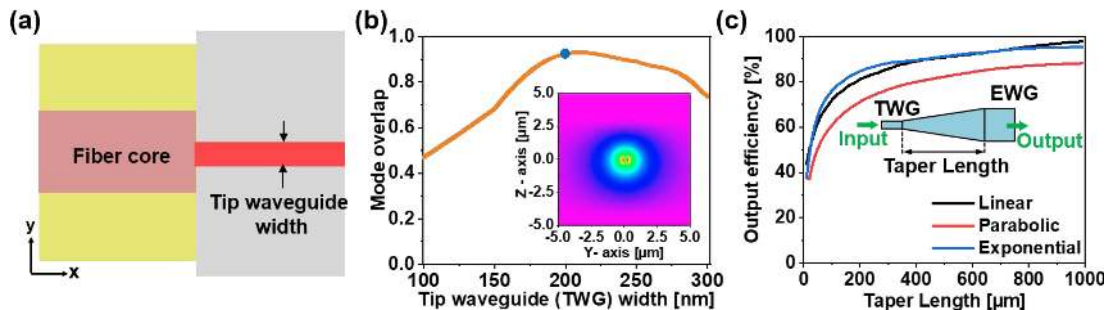

Fig. 2. (a) Schematic of a setup for calculating the mode overlap. (b) Mode overlap between the TWG and fiber for different TWG widths. The mode profile of a 200-nm TWG is shown in the inset exhibiting MFDs of 2.2 × 2.1 μm^2 along the y- and z-axes, respectively at λ = 1550 nm. (c) Output efficiencies as a function of the taper length, for different tapers connecting a 200-nm wide TWG to a 2-μm wide EWG.

The coupling efficiency of an edge coupler is primarily governed by two factors: taper design and taper tip-width. The taper should be carefully designed to efficiently guide the light to the tip waveguide with minimal loss, while the taper tip-width should be appropriately chosen to achieve superior mode overlap with the fiber. A pertinent value for the width of the tip waveguide was initially explored by observing the mode overlap [33] between the tip waveguide and fiber, as illustrated in Fig. 2(a). The refractive indices of Si_3N_4 and SiO_2 were approximately set to 1.97 and 1.44, respectively, considering that the variations in the refractive indices of the materials were below as small as 0.002 for wavelengths in the range of 1530 to 1630 nm. Fig. 2(b) shows the mode overlap integral as a function of the width of the tip waveguide. It is evident here that a width of 200 nm results in the highest mode overlap of approximately 0.94. For the chosen width of 200-nm, the fundamental transverse electric (TE) mode profile is shown in the inset of Fig. 2(b), which exhibits MFDs of 2.2 × 2.1 μm^2 along the horizontal (y-axis) and vertical (z-axis) directions, respectively. The mode profile confirmed that for a BOX as thick as 4 μm, the penetration of mode into the substrate was substantially suppressed. A simulation tool based on the beam propagation method (BPM), BeamPROP (Synopsys Inc.), was used for the design process. The 3D simulations were performed based on a nonuniform mesh scheme incorporating a nominal mesh size of as small as 10 nm, which was found to secure the convergence of the numerical calculations.
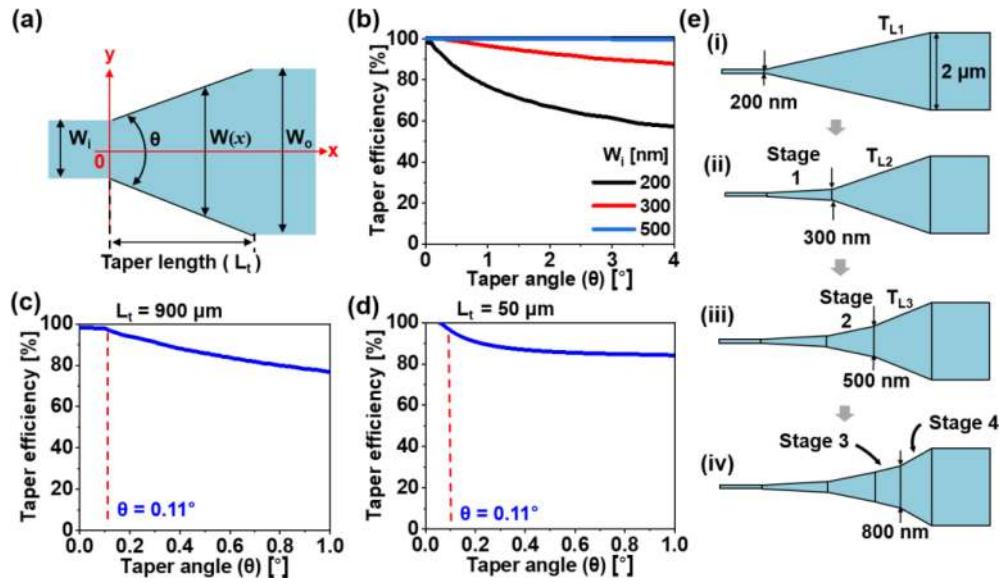
Fig. 3. (a) Schematic of a taper segment. (b) Impact of taper angle on the taper efficiency for varying W_i, where $W_o = 2$ μm. Taper efficiency as a function of the taper angle under $W_i = 200$ nm for (c) $W_o = 2$ μm and (d) $W_o = 300$ nm. (e) Design procedure of the proposed taper.

After determining the width of the tip waveguide, the taper segments were sequentially designed, beginning from the tip waveguide towards the end waveguide. To determine an optimal taper profile for the taper segments, the taper efficiencies of three taper profiles were inspected as a function of the taper length. As shown in the inset of Fig. 2(c), the efficiency of the taper connecting the 200-nm wide TWG to the 2-μm wide EWG was examined for the cases of linear, parabolic, and exponential profiles. The taper width at any position along the x-axis is given by $W(x) = W_i + (W_o - W_i)(x/L_t)^2$ and $W(x) = W_i + (W_o - W_i)\{(e^{x/L_t} - 1)/(e - 1)\}$ for the parabolic and exponential tapers, respectively. Here, W_i and W_o are the input and output widths of the taper, x is the x-axis coordinate, and L_t is the taper length. The exponential taper was observed to closely resemble the linear taper, from the perspective of the efficiency depending on the length. However, owing to its simple geometrical structure, the linear profile was practically favored for constructing the taper segments. A linear taper segment with an input width of W_i and output width of W_o is shown in Fig 3(a). The taper angle (θ) is calculated using $\theta = \arctan[(W_o - W_i)/L_t]$, while the width at any point along the x-axis can be calculated using $W(x) = W_i + [(W_o - W_i)x/L_t]$. Each taper segment constituting the proposed coupler was individually chosen by scrutinizing the maximum acceptable taper angle and the taper efficiency with respect to the end width of the taper. Here, the taper efficiency (E_{tpr}) is defined as the measure of optical power transmitted from W_i to W_o through the taper. As shown in Fig. 3(b), the effect of the taper angle on the taper efficiency (E_{tpr}) was investigated for the selected tip width W_i ranging between 200 nm and 500 nm, under $W_o = 2$ μm. It is evident that for narrow tapers with end widths below 500 nm, E_{tpr} is more susceptible to the variations in the taper angle due to their tenuous mode confinement. The mode confinement is deemed to be strengthened with an increase in the width of the end waveguide, thereby relaxing constraints on the taper angle. We could ultimately achieve a miniaturized taper consisting of multiple taper segments, where W_i for each segment was successively enlarged to shorten the corresponding taper length. The structural parameters corresponding to each taper segment were carefully chosen to maximize the overall taper efficiency (E_{tpr}) while keeping the footprint small. From the perspective of the mode confinement of individual taper segments, a threshold level of E_{tpr} equivalent to 97% was selected for widths below 500 nm, so as to minimize the excessively long footprint requirement. On the contrary, E_{tpr} above 99% was chosen for widths beyond 500 nm owing to their reinforced

TABLE 1
Structural Parameters and Efficiency of Single-Stage Tapers and the Proposed Multi-Stage Taper Segments That Supplanted Them

Design step	Single stage taper		Proposed multi-stage taper segment		Parameters	
	Transition (W_i to W_o)	Taper length (L_t)	Transition (W_i to W_o)	Taper length (L_t)	Taper angle (θ)	Taper efficiency (E_{tpr})
i	200 nm to 2 μm (T_{L1})	900 μm	200 nm to 300 nm (Stage 1)	50 μm	0.11°	97 %
ii	300 nm to 2 μm (T_{L2})	93 μm	300 nm to 500 nm (Stage 2)	11 μm	1.04°	97 %
iii	500 nm to 2 μm (T_{L3})	25 μm	500 nm to 800 nm (Stage 3)	5 μm	3.43°	99.9 %
iv	800 nm to 2 μm (T_{L4})	10 μm	800 nm to 2 μm (Stage 4)	10 μm	6.84°	99.9 %

mode confinement. All the taper segments that complied with the efficiency requirement, were appropriately allocated to the stages constituting the proposed coupler.

The proposed coupler was designed by considering a long adiabatic single-stage taper (T_{L1}) with $W_i = 200$ nm and $W_o = 2$ μm, as shown in Fig. 3(e-i). E_{tpr} corresponding to T_{L1} was calculated by varying the taper angle, as illustrated in Fig. 3(c). E_{tpr} drastically escalates with decreasing taper angle and saturates at $\sim 97\%$ for a taper length of 900 μm ($\theta = 0.11°$). A taper exhibiting an equivalent taper angle and a minimal footprint was selected to substitute T_{L1}. A short taper with a length of 50 μm (Stage 1), exhibiting $\theta = 0.11°$, yielded an equivalent E_{tpr} for $W_i = 200$ nm and $W_o = 300$ nm, as shown in Fig. 3(d). It is implied from Fig. 3(e-ii) that the short taper for Stage 1 needs to be appended to another taper (T_{L2}), whose width varies from 300 nm to 2 μm so as to serve as a legitimate substitute for the long taper T_{L1}. A similar iteration process was utilized to determine a short taper that could replace the cascaded taper (T_{L2}), which normally required a length of 93 μm ($\theta = 1.04°$). A short taper (Stage 2) with $W_i = 300$ nm linked to $W_o = 500$ nm produced an equivalent result under a taper length of 11 μm. The long taper (T_{L2}) was supplanted with Stage 2 taper in conjunction with another taper (T_{L3}), connecting $W_i = 500$ nm and $W_o = 2$ μm, as shown in Fig. 3(e-iii).

So far, the designed taper incorporated three taper segments. The first two segments (Stage 1 and Stage 2), which connected widths from 200 nm to 500 nm to result in a combined total length of 61 μm, were cascaded with a third segment (T_{L3}), which connected widths from 500 nm to 2 μm. The taper (T_{L3}), being 25 μm long, required a taper angle of $\theta = 3.43°$ to achieve the targeted maximum taper efficiency. Hence, the total length of the overall taper amounted to 86 μm. An extra iteration could reduce the length by 10 μm, leading to an overall length of 76 μm. Thus, according to the last iteration, T_{L3} was replaced by a taper segment joining widths between 500 nm and 800 nm (Stage 3), linked to another taper (T_{L4} or Stage 4), as shown in Fig. 3(e-iv). We also attempted to identify an ideal taper by further sectioning the existing four taper segments into 10 segments each. As a result, the width profile along the propagation direction could be reasonably modeled by an exponential curve as given by $W(x) = ae^{bx} + ce^{dx}$, where a, b, c and d are the fitting coefficients. However, further increment in the number of taper segments exerted only a slight impact on the overall footprint as well as the total efficiency. Consequently, a four-stage taper having a total length of 76 μm was finalized to replace the entire taper (T_{L1}). The overall design procedure is elaborated in Fig. 3(e), and all the structural parameters of the single-stage taper and the taper segments that supplanted them are tabulated in Table 1. It is worth noting that the designed taper segments satisfy the angular and coupling efficiency constraints, corresponding to the single-stage adiabatic taper. The spectral bandwidth and alignment tolerance of the cascaded taper structure depicted in Fig. 1 was validated through simulations.

3. Fabrication and Characterization of the Proposed Coupler

To characterize the designed multi-stage coupler, a suite of samples was manufactured on a 4-inch silicon wafer coated with a 4-μm thick BOX layer. The device was fabricated at Ligentec
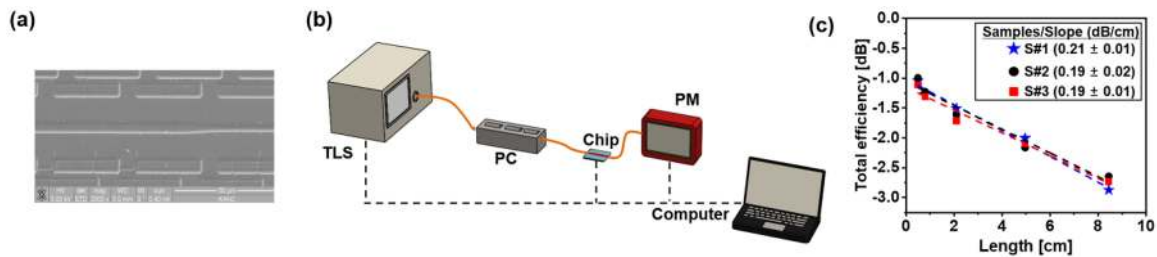
Fig. 4. (a) SEM image of the fabricated device. (b) Schematic of the measurement setup. (c) Measured total efficiencies of three fabricated samples (S#1, S#2 and S#3) with different lengths at $\lambda = 1550$ nm, with the slope indicating the propagation loss.

SA by adopting a photonic Damascene process, which has been reported to produce a Si_3N_4 film with thickness spanning from 0.1 μm to over 2 μm, incurring a propagation loss as low as 0.1 dB/cm [34]. A Si_3N_4 film with a thickness of 500 nm was formed atop the substrate via low-pressure chemical vapor deposition. Subsequently, the taper patterns, in conjunction with straight waveguides with lengths in the range of 5 mm to 10 cm, were lithographically prepared and etched according to the design. It must be noted that, only a single-step lithographic process was required to produce the pattern for the four-stage taper. A 3-μm thick SiO_2 layer was then deposited through plasma-enhanced chemical vapor deposition, which served as an upper cladding for the waveguides. The devices were initially manufactured on a reticle with dimensions of 22 × 22 mm^2, which was then diced into multiple smaller dies with a footprint of 5 × 11 mm^2. The input and output ports were positioned at the edge facets of the chip die, which were polished for efficient coupling. A scanning electron microscopy (SEM) image of the fabricated device is shown in Fig. 4(a). Fig.s 4(b) depicts the schematic of the experimental setup for assessing the performance of the fabricated device. Light from a tunable laser source (TLS) [81949A, Agilent] was fed into the prepared device via a polarization controller (PC) [STPC, KS Photonics] thereby setting the required state of polarization. Prior to coupling light from the fiber into the input facet of the device, the polarization at the input fiber tip was accurately calibrated to be either TE or transverse magnetic (TM) through a polarizer. The light emanating from the end facet of the device was coupled to an output fiber connected with an InGaAs photodiode [S154C, Thorlabs], which was tethered to a power meter (PM) [PM100D, Thorlabs]. A computer software was developed to operate the TLS, power meter used for recording the power spectrum, and the motorized stages used for controlling the input and output fibers.

To investigate the performance of the proposed coupler, a previously reported two-step method was adopted [15], [35]–[36]. The fiber-to-fiber coupling efficiency was first measured by directly aligning two decently cleaved fibers. Subsequently, to determine the fiber-chip-fiber coupling efficiency, the prepared device was placed in between the fibers and was carefully aligned, thus allowing light to travel from the input fiber into the chip through the input coupler and then exit via the output coupler into the output fiber. The difference between the fiber-to-fiber coupling and fiber-chip-fiber coupling efficiency was equal to the sum of fiber-to-chip coupling efficiency at both facets and the propagation loss. To examine the propagation loss, a set of waveguides with different lengths were evaluated in terms of the optical coupling at $\lambda = 1550$ nm. For the three sets of samples from different reticles on the same wafer, the measured total efficiencies were plotted in Fig. 4(c), signifying a propagation loss of 0.2 dB/cm. The results from all the samples were substantially consistent to justify their reproducibility. The propagation loss was then deducted to extract the coupling efficiency of the coupler at each facet. Regarding the simulated and measured results, the fiber-to-chip coupling efficiency is governed by the loss pertaining to the taper in conjunction with the mode overlap between the taper tip and fiber.

The simulated spectral response of the proposed coupler for the TE mode is shown in Fig. 5(a). For comparison, single-staged tapers of 76-μm length incorporating an exponential and parabolic
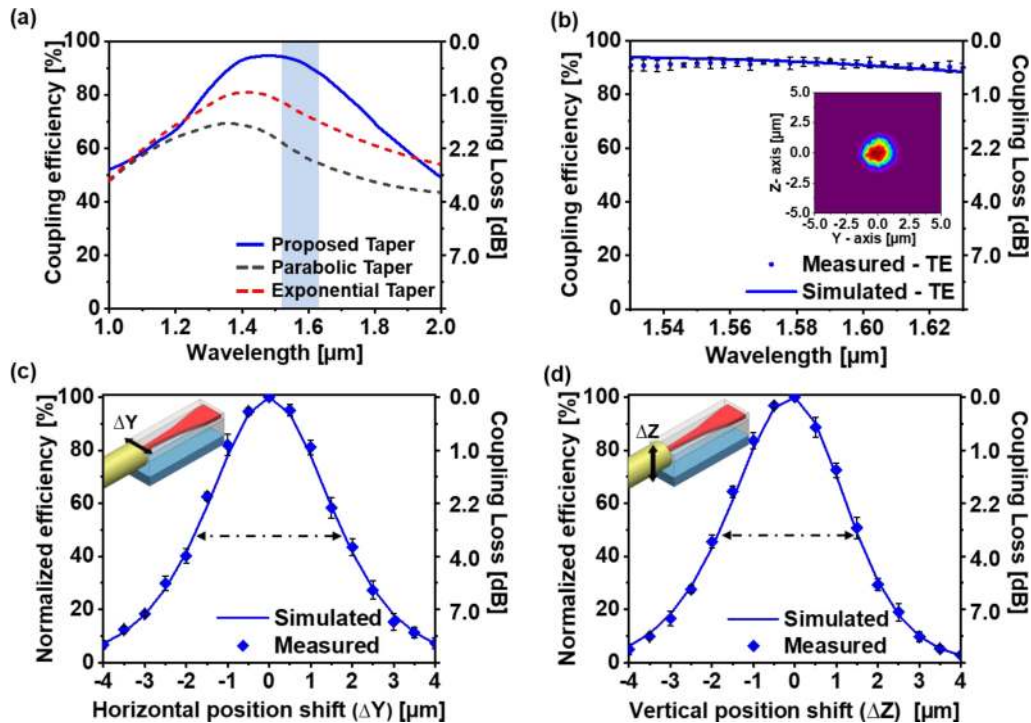
Fig. 5. (a) Simulated spectral response of the proposed multistage-taper (blue line) for TE mode; and the responses of a single-staged parabolic taper (dotted black line) and a single-staged exponential taper (red dotted line), each with a length of 76 μm. (b) Simulated and measured coupling efficiencies of the coupler over the C- and L-bands (1530–1625 nm). The inset shows the TE mode profile at the facet of the fabricated tip edge. (c) Horizontal and (d) vertical alignment tolerances of the proposed coupler at λ = 1550 nm. All the plotted results are based on the average of three measured data, with the error bar corresponding to the standard deviation.

taper profile were assessed via simulations, as shown in Fig. 5(a). The proposed coupler was observed to give rise to superior coupling efficiency compared to the other tapers with the equivalent length. The proposed coupler manifested a broadband operation with a 3-dB bandwidth of 965 nm, spanning λ = 1015–1980 nm. The experimental characterization was performed over a spectral regime spanning λ = 1530–1630 nm, covering both C and L bands, as shown by the blue highlighted region in Fig. 5(a).The experimentally measured coupling is as high as 92% at 1550-nm and beyond 90% in the whole measured spectral range, as presented in Fig. 5(b). For the three measurements performed on three samples from three different chip dies, the standard deviation corresponding to the entire spectrum is 1.48% on average, appropriately justifying the consistency of measurement. Further, the measured results show a good correlation with the simulated results, while the slight discrepancy between them may be attributed to the fabrication abnormalities associated with the slanted sidewall angle and the narrow tip width. To confirm that the measured data were not affected by stray light, the mode profile of the end facet was observed using a beam profiler (CinCAM-1202) equipped with a 60x objective lens. As shown in the inset of Fig. 5(b), the mode profile of the fabricated tip exhibited MFDs of 2.1 $\times$ 2.0 μm^2 along the horizontal (y-axis) and vertical (z-axis) directions, respectively. It was evident that the light beam was exclusively emanating from the waveguide, and no stray light was emitted through the cladding and substrate of the device. Additionally, no optical signal was captured by the beam profiler while scanning the input fiber, suggesting that the light was not directly transmitted from the input to the output fiber. Further, in order to explore the alignment tolerance of the device, one of the two end fibers was mechanically scanned, while the fibers at both the end facets were optimally aligned at λ = 1550 nm. As in the case of the coupling efficiency, three measurements were performed, and
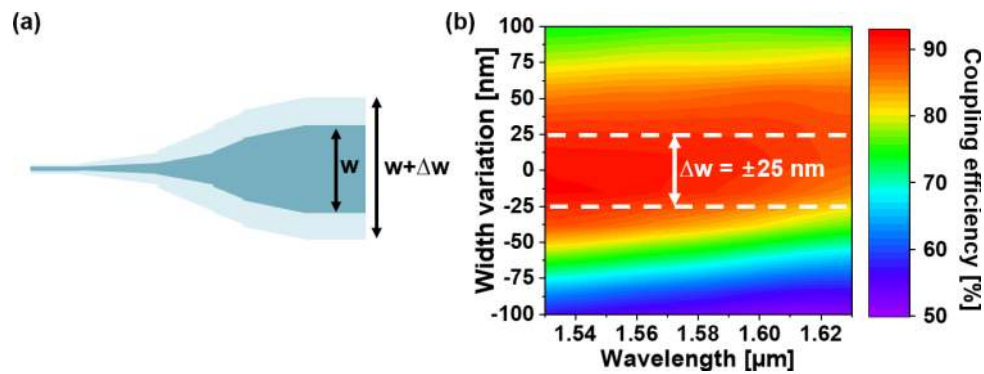
Fig. 6. (a) Schematic showing the variation in width associated with the fabrication tolerance. (b) Impact of the width variation on the coupling efficiency of the coupler for the TE mode.
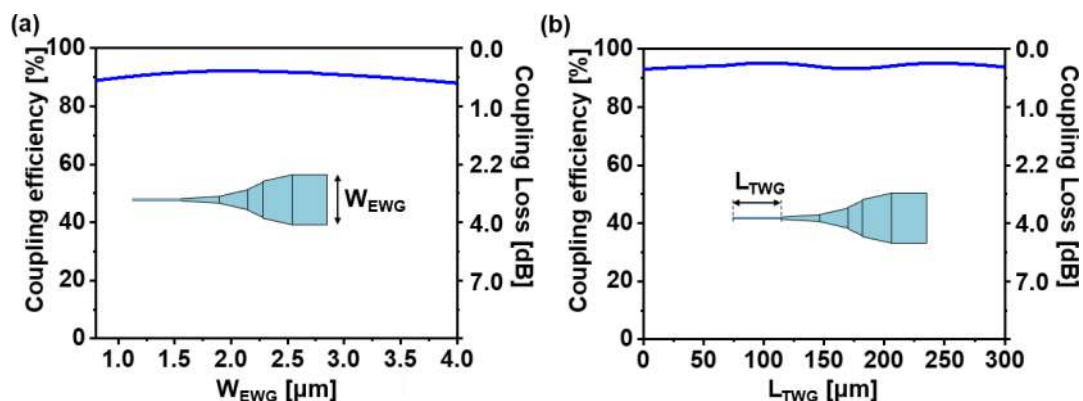

Fig. 7. Spectral response of the proposed coupler as a function of (a) end waveguide width and (b) length of the tip waveguide.

their average values were plotted in Figs. 5(c) and 5(d). The horizontal and vertical 3-dB alignment tolerances were 3.5 μm and 3.3 μm, respectively. Further, the performance of the fabricated device was also examined in regard to the fabrication tolerance. The coupling efficiency of the device was assessed in terms of the width variation (Δw) between -100 and $+100$ nm, as shown in Fig. 6(a). The results in Fig. 6(b) reveal that the coupling efficiency for the TE mode is hardly affected by variations in the taper width ranging up to ±25 nm, retaining efficiencies above 82% throughout the C and L bands.

Apart from its high coupling efficiency, remarkably tolerant alignment, and broadband spectral response, the proposed device exhibited additional attributes that cemented its excellent performance. In view of the width of the end waveguide corresponding to $W_{EWG} = 2$ μm, the proposed design could successfully accommodate W_{EWG} ranging between 1 μm and 4 μm, without affecting the length under a fixed tip width of 200 nm. This could be achieved by simply altering the angle of the last taper segment (Stage 4). As depicted in Fig. 7(a), the total coupling efficiency remains almost constant regardless of the variations in W_{EWG}, which can be used for applications based on wide waveguides like gyroscopes and accelerometers [37], [38]. Notably, the end of the taper tip is elongated for improving the cleaving tolerance, and the length of the tip waveguide (L_{TWG}) negligibly affects the performance, as shown in Fig. 7(b).

For the proposed device, additional simulations and experiments were also performed to verify its potential operation for the TM mode. The simulations and experiments for the TM mode were performed using the same design parameters as in the case of the TE mode. Fig. 8(a) shows
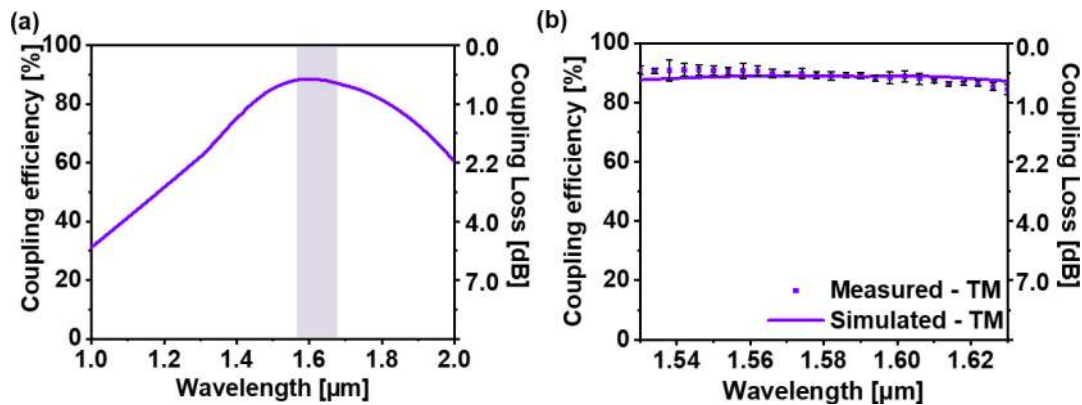
Fig. 8. (a) Calculated spectral response for the TM mode and (b) measured spectral response in the C and L spectral bands, where error bars represent the standard deviation.

TABLE 2

Comparison of Various Types of Edge Couplers in Si_3N_4 Platform

Reference	Total length	Coupling efficiency		3-dB alignment tolerance		Si_3N_4 thickness/ lithography
		TE mode	TM mode	Horizontal	Vertical	
[15]	500 µm	98%	-	3.6 µm	3.5 µm	100 nm / a single step
[17]	151 µm	89%	-	-	-	300 nm–150 nm / double steps
Current work	76 µm	92%	88%	3.5 µm	3.3 µm	500 nm/ a single step

the simulated spectral coupling response for the TM mode in the regime spanning $\lambda = 1\text{–}2$ µm. As shown in Fig. 8(b), the measured coupling efficiency is above 85% throughout the C and L bands, reaching as high as 88% at 1550 nm wavelength. Similar to the case of a TE mode, the measurements were performed on three samples and had an average standard deviation of 1.46%, validating the consistency of the measured results. The proposed coupler was primarily designed for the TE mode rather than the TM mode. Hence, the coupling efficiency for the TM mode can be further improved by considering the corresponding mode characteristics. Further, it is noted that the performance of the device for the TM mode is reasonable considering that its efficiency exceeds 85% throughout the C and L bands, as shown in Fig. 8(b). The proposed coupler can be readily engineered to render a polarization-insensitive operation, by optimizing the aspect ratio of the tip waveguide [11]. Lastly, the proposed coupler has also been compared with other edge couplers reported in Si_3N_4 platform in terms of the footprint, coupling efficiency, and alignment tolerance, as tabulated in Table 2. It is evident that the proposed device exhibits the shortest footprint among all, featuring a comparable coupling efficiency and alignment tolerance.

4. Conclusion

A substantially miniaturized edge coupler was successfully demonstrated by cascading a series of taper segments with meticulously determined taper angles, which were obtained by segmenting a long adiabatic taper. The taper segments were allocated to the four stages yielding a short length of 76 µm. The coupling efficiency of the proposed coupler was as high as 92% and 88% for the TE and TM modes at 1550-nm wavelength, respectively. An excellent agreement was observed between the simulated and measured results. The proposed device exhibited enhanced cleaving tolerance by utilizing an elongated tip waveguide. Further, a high alignment tolerance was observed in both horizontal and vertical directions. The proposed coupler was primarily designed for a high NA fiber with mode size of 4.0 µm at a wavelength of 1550 nm. Moreover, the proposed design approach

is also applicable to a standard SMF fiber if it is spliced to a high-NA fiber. In addition to realizing a compact footprint, the proposed coupler may readily adapt to any waveguide widths without sacrificing the length and the coupling efficiency. Although it was primarily targeted for a Si_3N_4 platform, the proposed coupler design exhibits immense potential for fiber-to-chip and chip-to-chip couplings based on different platforms as well. Thus, it may serve as an excellent reference for further explorations to achieve compact components and to realize high-density photonic integrated circuits.

Acknowledgment

References

[1] J. F. Bauters *et al.*, "Ultra-low-loss high-aspect-ratio Si_3N_4 waveguides," *Opt. Exp.*, vol. 19, no. 4, pp. 3163–3174, Feb. 2011.

[2] D. J. Moss, R. Morandotti, A. L. Gaeta, and M. Lipson, "New CMOS-compatible platforms based on silicon nitride and hydex for nonlinear optics," *Nat. Photon.*, vol. 7, no. 8, pp. 597–607, Jul. 2013.

[3] P. Muñoz *et al.*, "Silicon nitride photonic integration platforms for visible, near-infrared and mid-infrared application," *Sensors*, vol. 17, no. 9, Sep. 2017, Art. no. 2088.

[4] R. Marchetti, C. Lacava, L. Carroll, K. Gradkowski, and P. Minzioni, "Coupling strategies for silicon photonics integrated chips," *Photon. Res*, vol. 7, no. 2, pp. 201–239, Feb. 2019.

[5] Y. Zhu *et al.*, "Ultra-compact silicon nitride grating coupler for microscopy systems," *Opt. Exp.*, vol. 25, no. 26, pp. 33297–33304, Dec. 2017.

[6] J. C. C. Mak, W. D. Sacher, H. Ying, X. Luo, P. G.-Q. Lo, and J. K. S. Poon, "Multi-layer silicon nitride-on-silicon polarization-independent grating couplers," *Opt. Exp.*, vol. 26, no. 23, pp. 30623–30633, Nov. 2018.

[7] G. Son, S. Han, J. Park, K. Kwon, and K. Yu, "High-efficiency broadband light coupling between optical fibers and photonic integrated circuits," *Nanophotonics*, vol. 7, no. 12, pp. 1845–1864, Oct. 2018.

[8] O. Mitomi, K. Kasaya, and H. Miyazawa, "Design of a single-mode tapered waveguide for low-loss chip-to-fiber coupling," *IEEE J. Quantum Electron.*, vol. 30, no. 8, pp. 1787–1793, Aug. 1994.

[9] J. Zou *et al.*, "Short and efficient mode-size converter designed by segmented-stepwise method," *Opt. Lett.*, vol. 39, no. 21, pp. 6273–6276, Nov. 2014.

[10] T. Mizuno *et al.*, "Compact and low-loss arrayed waveguide grating module with tolerance-relaxed spot-size converter," *IEEE Photon. Technol. Lett.*, vol. 15, no. 2, pp. 239–241, Feb. 2003.

[11] P. Cheben *et al.*, "Broadband polarization independent nanophotonic coupler for silicon waveguides with ultra-high efficiency," *Opt. Exp.*, vol. 23, no. 17, pp. 22553–22563, Aug. 2015.

[12] Y. Liu *et al.*, "Adiabatic and ultracompact waveguide tapers based on digital metamaterials," *IEEE J. Sel. Topics Quantum Electron.*, vol. 25, no. 3, May/Jun. 2019, Art. no. 4700106.

[13] S. H. Tao, J. Song, Q. Fang, M. B. Yu, G. Q. Lo, and D. L. Kwong, "Improving coupling efficiency of fiber-waveguide coupling with a double-tip coupler," *Opt. Exp.*, vol. 16, no. 25, pp. 20803–20808, Dec. 2008.

[14] N. Kohli, M. Ménard, and W.N. Ye, "Efficient TE/TM spot-size converter for broadband coupling to single mode fibers," *OSA Continuum*, vol. 2, no. 8, pp. 2428–2438, Aug. 2019.

[15] T. Zhu, Y. Hu, P. Gatkine, S. Veilleux, J. B.-Hawthorn, and M. Dagenais, "Ultrabroadband high coupling efficiency fiber-to-waveguide coupler using Si_3N_4/SiO_2 waveguides on silicon," *IEEE Photon. J.*, vol. 8, no. 5, Oct. 2016, Art. no. 7102112.

[16] P. Sethi, R. Kallega, A. Haldar, and S. K. Selvaraja, "Compact broadband low-loss taper for coupling to a silicon nitride photonic wire," *Opt. Lett.*, vol. 43, no. 14, pp. 3433–3436, Jul. 2018.

[17] J. Fernández, R. Baños, D. Doménech, C. Domínguez, and P. Muñoz, "Low-loss inverted taper edge coupler in silicon nitride," *IET Optoelectron*, vol. 13, no. 2, pp. 62–66, Mar. 2019.

[18] L. Xu *et al.*, "Polarization independent adiabatic 3-dB coupler for silicon-on-insulator," in *Proc. Conf. Lasers Electro-Optics*, paper SF1I.5, 2017.

[19] Y. Wang *et al.*, "Polarization-independent mode-evolution-based coupler for the silicon-on-insulator platform," *IEEE Photon. J.*, vol. 10, no. 3, Jun. 2018, Art. no. 4900410.

[20] L. Xu *et al.*, "Compact high-performance adiabatic 3-dB coupler enabled by subwavelength grating slot in the silicon-on-insulator platform," *Opt. Exp.*, vol. 26, no. 23, pp. 29873–29885, Nov. 2018.

[21] H. Yun, L. Chrostowski, and N. A. F. Jaeger, "Ultra-broadband 2×2 adiabatic 3 dB coupler using subwavelength-grating-assisted silicon-on-insulator strip waveguides," *Opt. Lett.*, vol. 43, no. 8, pp. 1935–1938, Apr. 2018.

[22] D. Mao *et al.*, "Adiabatic coupler with design-intended splitting ratio," *J. Lightw. Technol.*, vol. 37, no. 24, pp. 6147–6155, Oct. 2019.

[23] C. Sun, Y. Yu, M. Ye, G. Chen, and X. Zhang, "An ultra-low crosstalk and broadband two-mode (de)multiplexer based on adiabatic couplers," *Sci. Rep.*, vol. 6, Dec. 2016, Art. no. 38494.

[24] Z. Zhang, Y. Yu, and S. Fu, "Broadband on-chip mode-division multiplexer based on adiabatic couplers and symmetric Y-junction," *IEEE Photon. J.*, vol. 9, no. 2, Apr. 2017 Art. no. 6600406.

[25] D. Guo and T. Chu, "Silicon mode (de)multiplexers with parameters optimized using shortcuts to adiabaticity," *Opt. Exp.*, vol. 25, no. 8, pp. 9160–9170, Apr. 2017.

[26] L. Xu *et al.*, "Ultra-broadband and compact two-mode multiplexer based on subwavelength-grating-slot-assisted adiabatic coupler for the silicon-on-insulator platform," *J. Lightw. Technol.*, vol. 37, no. 23, pp. 5790–5800, Sep. 2019.

[27] X. Tu, M. Li, J. Xing, H. Fu, and D. Geng, "Compact PSR based on an asymmetric bi-level lateral taper in an adiabatic directional coupler," *J. Lightw. Technol.*, vol. 34, no. 3, pp. 985–991, Dec. 2016.

[28] C. Sun, Y. Yu, G. Chen, and X. Zhang, "A low crosstalk and broadband polarization rotator and splitter based on adiabatic couplers," *IEEE Photon. Technol. Lett.*, vol. 28, no. 20, pp. 2253–2256, Oct. 2016.

[29] Y. Yin, Z. Li, and D. Dai, "Ultra-broadband polarization splitter-rotator based on the mode evolution in a dual-core adiabatic taper," *J. Lightw. Technol.*, vol. 35, no. 11, pp. 2227–2233, Feb. 2017.

[30] H. -C. Chung and S. -Y. Tseng, "Ultrashort and broadband silicon polarization splitter rotator using fast quasiadiabatic dynamics," *Opt. Exp.*, vol. 26, no. 8, pp. 9655–9665, Apr. 2018.

[31] R. F. Dangel *et al.*, "Polymer waveguides enabling scalable low-loss adiabatic optical coupling for silicon photonics," *IEEE J. Sel. Topics Quantum Electron.*, vol. 24, no. 4, Jul./Aug. 2018, Art. no. 8200211.

[32] P. Yin *et al.*, "Low connector-to-connector loss through silicon photonic chips using ultra-low loss splicing of SMF-28 to high numerical aperture fibers," *Opt. Exp.*, vol. 27, no. 17, pp. 24188–24193, Aug. 2019.

[33] S. Zuoming, S. Ningfang, J. Jing, S. Jingming, and M. Pan, "Low loss fusion splicing polarization-maintaining photonic crystal fiber and conventional polarization-maintaining fiber," *Opt. Fiber Technol.*, vol. 18, no. 6, pp. 452–456, Dec. 2012.

[34] M. H. P. Pfeiffer *et al.*, "Photonic damascene process for low-loss, high-confinement silicon nitride waveguides," *IEEE J. Sel. Topics Quantum Electron.*, vol. 24, no. 4, Jul. Aug. 2018, Art. no. 6101411.

[35] L. Chen, C. R. Doerr, Y.-K. Chen, and T.-Y. Liow, "Low-loss and broadband cantilever couplers between standard cleaved fibers and high-index-contrast Si3N4 or Si waveguides," *IEEE Photon. Technol. Lett.*, vol. 22, no. 23, pp. 1744–1746, Dec. 2010.

[36] J. Cardenas, C. B. Poitras, K. Luke, L.-W. Luo, P. A. Morton, and M. Lipson, "High coupling efficiency etched facet tapers in silicon waveguides," *IEEE Photon. Technol. Lett.*, vol. 26, no. 23, pp. 2380–2382, Dec. 2014.

[37] J. Yao *et al.*, "Compact spot-size converter for low-loss coupling and miniaturization of interferometric fiber optic gyroscopes," *Opt. Comm.*, vol. 452, pp. 321–326, Dec. 2019.

[38] F. Wan, G. Qian, R. Li, J. Tang, and T. Zhang, "High sensitivity optical waveguide accelerometer based on fano resonance," *Appl. Optics*, vol. 55, no. 24, pp. 6644–6648, Aug. 2016.